Article

Applied Spectroscopy

Applied Spectroscopy
2016, Vol. 70(6) 962–971

DOI: 10.1177/0003702816641261
asp.sagepub.com

SAGE

A Light-Emitting Diode- (LED-) Based Absorption Sensor for Simultaneous Detection of Carbon Monoxide and Carbon Dioxide

Kyle Thurmond[1], Zachary Loparo[1], William Partridge[2], and Subith S. Vasu[1,3]

Abstract

A sensor was developed for simultaneous measurements of carbon monoxide (CO) and carbon dioxide (CO_2) fluctuations in internal combustion engine exhaust gases. This sensor utilizes low-cost and compact light-emitting diodes (LEDs) that emit in the 3–5 μm wavelength range. An affordable, fast response sensor that can measure these gases has a broad application that can lead to more efficient, fuel-flexible engines and regulation of harmful emissions. Light emission from LEDs is spectrally broader and more spatially divergent when compared to that of lasers, which presented many design challenges. Optical design studies addressed some of the non-ideal characteristics of the LED emissions. Measurements of CO and CO_2 were conducted using their fundamental absorption bands centered at 4.7 μm and 4.3 μm, respectively, while a 3.6 μm reference LED was used to account for scattering losses (due to soot, window deposits, etc.) common to the three measurement LEDs. Instrument validation and calibration was performed using a laboratory flow cell and bottled-gas mixtures. The sensor was able to detect CO_2 and CO concentration changes as small as 30 ppm and 400 ppm, respectively. Because of the many control and monitor species with infra-red absorption features, which can be measured using the strategy described, this work demonstrates proof of concept for a wider range of fast (250 Hz) and low-cost sensors for gas measurement and process monitoring.

Keywords

Absorption spectroscopy, carbon monoxide, CO, carbon dioxide, CO_2, light emitting diodes, LEDs, mid-infrared, MIR

Date received: 30 June 2015; accepted: 31 August 2015

Introduction

Liquid fuel usage is projected to increase by 38% from 2010 to 2040, with the transportation sector accounting for 63% of the total increase.[1] In order to meet increasingly stringent emissions regulations and to improve overall engine efficiency, new combustion methodologies, including advanced use of exhaust gas recirculation (EGR) are being explored.[2] The nature of the intake and exhaust both affect and reflect engine performance and combustion chemistry. Spatial and temporal variations in the intake air–EGR mixture can contribute to combustion non-uniformities, which reduce engine efficiency and contribute to increased production of regulated exhaust gas emissions.[3]

A sensor that can simultaneously monitor carbon monoxide (CO) and carbon dioxide (CO_2) will benefit enhanced emissions- and combustion-control development. Carbon monoxide is a primary product of incomplete combustion that can be used to indicate combustion efficiency; it is also toxic to humans and animals, and regulated by the US Environmental Protection Agency. Carbon dioxide is a product of complete combustion and is commonly used to quantify intake EGR levels; it is also a critical greenhouse gas and, along with CO, is a measure of combustion completion and total exhaust carbon output. Therefore, time-resolved knowledge of CO and CO_2 exhaust

[1]Center for Advanced Turbomachinery and Energy Research, Mechanical and Aerospace Engineering, University of Central Florida, Orlando, USA
[2]Fuels, Engines and Emissions Research Center, Oak Ridge National Laboratory, Oak Ridge, USA
[3]Florida Space Institute, University of Central Florida, Orlando, USA

Corresponding author:
Subith S. Vasu, University of Central Florida, 4000 Central Florida Blvd, Bldg 40-307, Orlando, FL 32816 USA.
Email: subith@ucf.edu

concentrations will aid in improving combustion strategies, control, and efficiency, and promote the transition to a cleaner energy infrastructure.

This work describes development and evaluation of a light-emitting diode (LED) based absorption sensor for simultaneous detection of the important CO and CO_2 exhaust gas species. Laser-based absorption measurement strategies have been developed extensively in combustion and propulsion related research, and enable non-intrusive, fast, time-resolved, precise, and accurate measurements of gas composition, temperature, velocity, and pressure.[4–7] However, the cost and complexity of laser-based systems limits their broader applicability beyond the laboratory, development, and certain industrial settings; specifically, they cannot provide a practical solution for automotive on-board diagnostics (OBD) and control. Light-emitting diodes present a potential solution for the development of sensors that are sufficiently cost-effective and rugged for practical on-board automotive applications. The design and methods discussed here may be applied to developing a range of low-cost sensors for measuring a variety of species. Figure 1 shows the spectral absorption features of several important gases within the spectral range of mid-infrared (MIR) LEDs (LED from Ioffe Institute/MIRDOG, Russia).[8]

The sensor described here has many benefits compared to existing commercially available sensors; these include response time, cost, size, applicability to integrated OBD systems, and suitability for in situ probe measurements versus extractive sampling. There currently exist two main categories of commercial non-dispersive infrared (NDIR) sensors for monitoring CO and CO_2. The first category includes small, compact sensors used primarily for monitoring manufacturing processes and in heating, ventilating, and air-conditioning (HVAC) systems. While being compact, these sensors have slow response times, ranging from 0.5 s to 20 s, and most do not measure both CO and CO_2 simultaneously. The second category of commercial sensors includes large laboratory systems (e.g., Horiba MEXA-7100FX) for making time-resolved measurements via extractive sampling; while these are routinely applied to engine research, they are bulky, not adaptable for probe-based measurements, and expensive. Neither of these types of sensors are suitable for on-board diagnostics, due to their slow response time, large size, and power requirements. Commercial systems exist (e.g., Horiba OBS-200) for on-road measurements of CO and CO_2 using NDIR; however, these are large (about 60 kg), primarily intended for development, and do not provide a diagnostic pathway for on-vehicle OBD integration. The sensor developed in this work provides fast, simultaneous measurements of CO and CO_2 in a compact and inexpensive package. Based on its similarity to a separately developed CO_2 sensor[9] that has been configured with a remote-probe sample interface

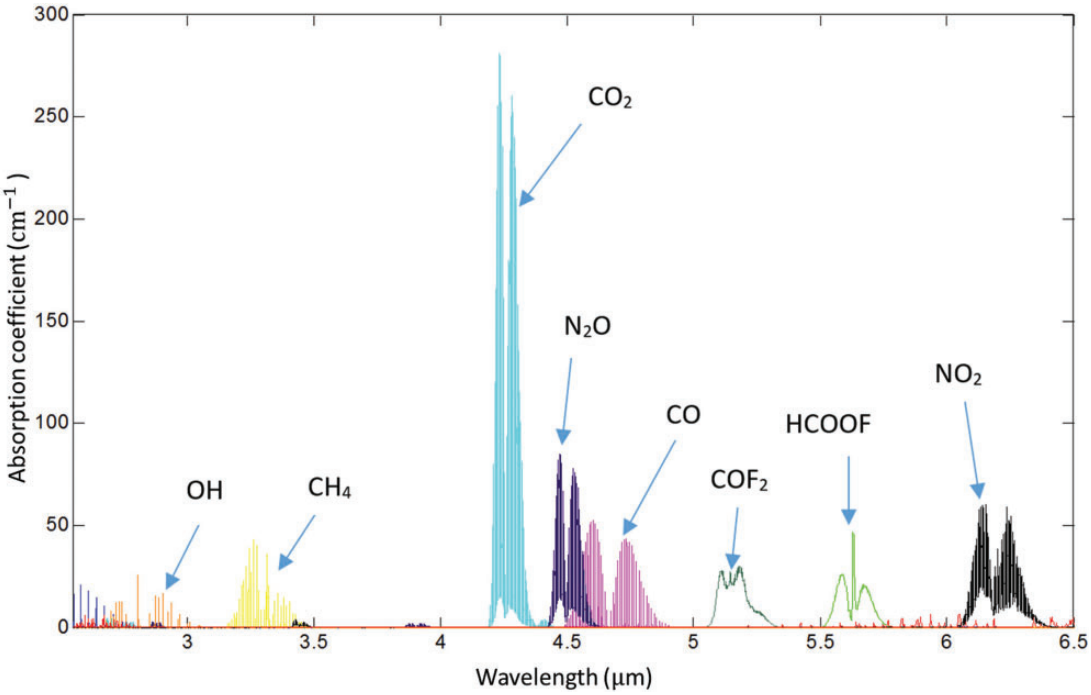

Figure 1. Absorption features of OH, H_2O, CH_4, CO_2, N_2O, CO, COF_2, HCOOF, and NO_2 in the MIR range. Although H_2O has absorption features throughout the indicated MIR range, because they have sufficiently small magnitude in the probed region, associated interference is practically negligible.

(versus extractive sampling) and applied for on-engine measurements, the sensor described here is expected to have these same capabilities. In summary, the sensor offers unique advantages compared to existing commercial CO and CO_2 sensors, is compact, inexpensive, configurable for probe-based measurements, applicable to on-engine measurements, and provides a pathway for the development of OBD sensors and other applications requiring these sensor characteristics, such as aviation and space exploration.

Theory

Absorption spectroscopy can be used to quantify the properties of a target molecular species via its characteristic absorption spectrum; these properties include concentration, temperature, and pressure. For species concentration measurements, light of a wavelength overlapping that of the targeted species' absorption spectra is directed through a gas. The light attenuation, due to absorption, is measured by comparing the incident and transmitted radiation, and is related to the target species' concentration. Monochromatic absorption spectroscopy follows the Beer–Lambert law, which relates the attenuation to the properties of light and adsorbing species; specifically, the ratio of the transmitted irradiance I (W cm^{-2}) to the incident irradiance I_0 (W cm^{-2}) when a spectrally narrow radiation at frequency ν (cm^{-1}) is directed through a gas medium. Broad spectrum absorption in the linear regime can be represented by summation spectrally integrated version of Beer's law

$$T = \left(\frac{I}{I_0}\right) = \int E_\lambda F_\lambda \exp(-k_\lambda L)\mathrm{d}\lambda \qquad (1)$$

where T (is the transmissivity, E_λ (unitless) is the spectral emissive profile of the LED source, F_λ (unitless) is the spectral transmissivity profile of the filter, k_λ (cm^{-1}) is the spectral absorption coefficient, and L (cm) is the absorption path length through the gas. The spectral absorption coefficient is defined as the product $k_\lambda = S_\lambda\ \phi_\lambda P x_i$ where S_λ ($cm^{-2}atm^{-1}$) is the line strength, ϕ (cm) the line–shape function, P (atm) is the total pressure, and x_i the mole fraction of the absorbing species. For this study, line strength values were determined from the HITRAN 2012 database, which provides a compilation of spectroscopic parameters used to predict and simulate the transmission of light in the atmosphere.[8]

For broadband absorption, many hundreds or thousands of individual absorption transitions may exist within the probed spectral region, which can lead to mixed-regime absorbance beyond the linear regime absorbance described by Eq. 1; i.e., stronger transitions may begin to saturate at certain CO and/or CO_2 concentrations while weaker transitions may remain in the linear regime. As will be seen, this creates a nonlinear response above a characteristic concentration where the major absorption transitions move from a linear to a saturated regime. Yoo et al.[9] discuss the curves-of-growth theory, typically applied in stellar atmosphere spectroscopy, as a potential model for such mixed-regime absorbance. In the analysis presented here, curves of growth are used to estimate line shape parameters as the spectral resolution is not sufficient to resolve individual transitions, and mixed-regime absorption certainly occurs (see Figure 6).

The line-strength S of a specific absorption transition can is a function of temperature and can be expressed as

$$S(T) = S(T_0)\frac{Q(T_0)}{Q(T)}\left(\frac{T_0}{T}\right)\exp\left[-\frac{hcE''}{k}\left(\frac{1}{T}-\frac{1}{T_0}\right)\right]\left[1-\exp\left(\frac{-hc\nu_0}{kT}\right)\right]\left[1-\exp\left(\frac{-hc\nu_0}{kT_0}\right)\right]^{-1} \qquad (2)$$

where $Q(T)$ is the partition function, E'' (cm^{-1}) the lower-state energy for the transition, ν_0 (cm^{-1}) is the transition's line-center frequency, T_0 (K) is the reference temperature corresponding to the reference line-strength $S(T_0)$, h is Planck's constant, c is the speed of light, and k is Boltzmann's constant.

Design

This sensor uses three LEDs to cover three different wavelength regions: a reference LED (I_0 in Beer's law) centered near 3.6 μm, one near 4.2 μm for detecting CO_2, and one near 4.7 μm for detecting CO. Figure 2 shows the normalized spectral profiles of these LEDs overlaid with the absorption features of CO and CO_2; it is clear from Figure 2 that the LEDs are spectrally broader than the individual absorption transitions, and that the associated measurements will be the integral of absorption from many individual lines in the indicated bands. Figure 2 also shows the spectral profiles of source-specific bandpass filters selected to narrow the bandwidth of the LEDs; these reduce spectral overlap between the three LEDs, and associated cross-interference. To achieve a steadier and consistent output performance over long time periods, each LED was individually temperature controlled (to $-10 \pm 0.2^{\circ}$C) using a two-stage thermal electric cooler (TEC).

Using a single detector for the three LED signals reduces instrument cost and complexities associated with multiple detectors; e.g., accounting for detector-specific response, dark current, noise, and other characteristics. This single-detector approach requires the three LEDs to be combined into a single measurement beam. The LEDs were individually collimated, filtered with the appropriate bandpass filters, and combined using two pellicle beam splitters as shown in Figure 3. The output of each LED was modulated at a unique frequency by a dedicated function generator,

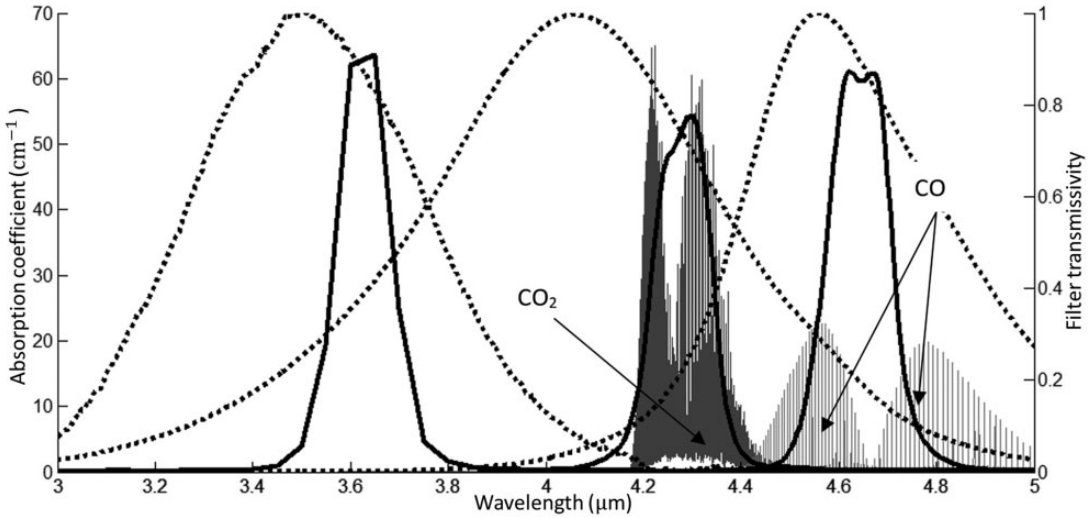

Figure 2. Normalized spectral profiles of the LEDs (dashed lines) and filters (solid lines). The absorption features of CO_2 and CO are shown (296 K) to illustrate spectral overlap between the LED emission, filter transmission, and absorption features.

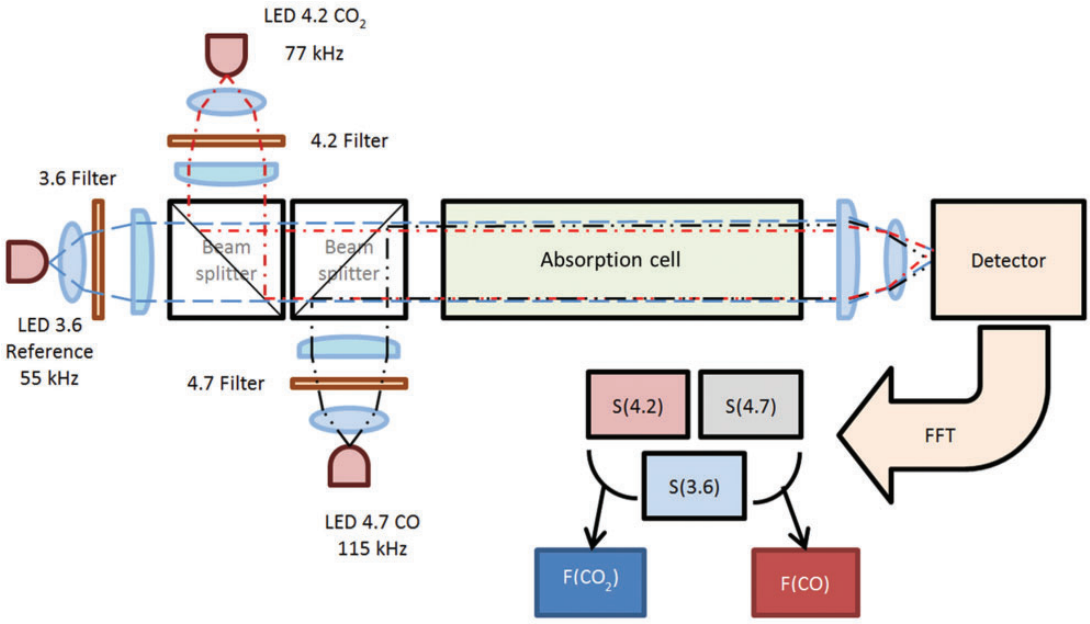

Figure 3. Sensor hardware and processing schematic including measurement flow cell.

using a square-wave unity-duty-cycle function; i.e., the 3.6 μm, 4.2 μm, and, 4.7 μm LEDs were modulated at 55 kHz, 77 kHz, and 115 kHz, respectively. The signal corresponding to each LED was determined from the Fourier transform of the combined single-detector signal as that at the corresponding modulation frequency. A Vigo Systems S.A. (Poland) three-stage TEC photovoltaic detector (model PVI-3TE-5) with an STCC-04 TEC controller (also Vigo Systems S.A., Poland) was used. This detector has a fast response and high sensitivity to radiation between 3 μm and 5 μm.

In order to optimize sensor performance, the spatially extended incoherent LED emission must be carefully coupled into and within the system. Optical-design software (Radiant ZEMAX)[10] allowed simulation of the entire sensor optical system, and was used to optimize the optical configuration. Figure 4 shows a simulation of the 3.6 μm LED as it is nominally collimated, transmitted through the beam-combining optics and measurement cell, and focused onto the detector.

The LED beams were nominally collimated to minimize signal loss from vignetting or clipping by hardware surfaces

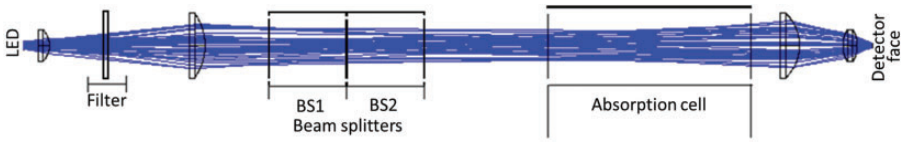

Figure 4. Simulation of the entire beam path for the 3.6 μm LED emission, which has the longest optical path. The beam splitters and absorption cell are drawn with approximate proportions for reference only.

during its travel through the sensor system; two plano-convex lenses (20 mm and 50 mm focal length CaF_2 lenses from Thorlabs) produced a semi-collimated beam with a working diameter (i.e., between the collimating and focusing lens sets) of approximately 12.7 mm. Following transmission through the measurement cell, a plano-convex lens coupled with a bi-convex lens (40 mm and 15 mm focal length CaF_2 lenses, respectively) were used to focus the combined three LED beams onto the 1 mm^2 square detector; i.e., although each LED has a dedicated collimating lens set, they have a common focusing lens set as indicated in Figure 3. Using the optical design software, we estimate that only approximately 1/3 of the LED emission is captured by the detector, reflecting the challenge of collimating and focusing the emission of spatially extended incoherent sources onto a small area. Even with these significant losses, we demonstrate significant instrument performance, as described below. Future work will focus on optimizing the optics, with the potential of tripling the signal and realizing corresponding diagnostic benefits regarding signal-to-noise ratio (SNR), temporal resolution, and detection limit.

Evaluation

The sensor performance was evaluated using neat gas mixtures to quantify species response factors, noise and detection limits, and cross interferences. The flowing measurement cell (see Absorption Cell in Figure 3) was constructed from PVC tubing, with sapphire windows, an 8 cm long absorption path length, and tubing connectors on each end to allow flow of the measurement gases. During evaluation and applications, the sensor was placed in an N_2-purged enclosure to eliminate ambient CO and CO_2 from the free-space optical train and errors due to additional light absorption outside the measurement cell. Neat bottled gas standards and a ten-point gas divider (STEC SGD-710 C) were used to control the measurement gas composition; the standards included 1% CO_2, 10% CO_2, and 4% CO, all in N_2 balance. A secondary rotameter pair were used for some of the cross-sensitivity studies. Single-gas calibration curves were measured by diluting the standards with ultra-high purity nitrogen; CO_2 was stepped from 0% to 1% in 0.1% intervals, and from 0% to 10% in 1% intervals, and CO was stepped from 0% to 4% in 0.4% intervals. Two methods were used to evaluate cross-interference between CO_2 and CO. In the first method, the primary standard was varied as described for the single-gas calibrations, using the gas divider and N_2 diluent, and combined with an N_2-diluted mixture of the secondary standard using the rotameter pair; i.e., when CO_2 was the primary standard, CO was the secondary, and vice versa; and the concentration of the secondary standard remained constant throughout all of the measurements. In the second method, the CO_2 and CO mirrored each other between zero and span levels by using the gas divider with CO used as the 'standard,' and CO_2 as the diluent; e.g., as CO_2 was stepped from 0–10% while CO was stepped from 4–0%. Two measurements were taken at each gas composition setting: one while stepping up the concentration of the standard and one while stepping down; lack of hysteresis between the two data sets confirmed that the cell reached steady state at each composition element of the calibration scan.

The analysis procedure provides for a 1 kHz (1 ms) measurement rate. For each measurement, the detector signal was recorded at 10^6 Hz for 1 s to obtain 10^6 samples. The data was split into 1000 time bins, each containing 1000 data points, and a fast Fourier transform (FFT) was performed on each bin in order to determine the signals (irradiance surrogate) from the three LEDs. After normalizing the two measurement LED signals using the reference LED signal, the absorbance values were calculated as per Eq. 1, but including a factor to account for differing optical losses between the various LED sources; i.e., the absorbance was calculated as $-\mathrm{In}\left((I_{4.2}/I_{3.6})/c_{\mathrm{CO_2}}\right)$ for CO_2 and $-\mathrm{In}((I_{4.7}/I_{3.6})/c_{\mathrm{CO}})$ for CO, where $c_{\mathrm{co_2}}$ and c_{co} are the loss factors determined from measurement of a non-absorbing N_2 sample. This analysis procedure provided for simultaneous CO_2 and CO measurements at 10^3 Hz. For the steady-state measurements, the standard deviation between the 1000 bins was used to quantify measurement uncertainty. Because the analysis procedure provides for a measurement rate of 10^3 Hz, the sensor is theoretically able to record fluctuations in absorbance of up to 500 Hz (the Nyquist frequency) without aliasing, and practically able to accurately resolve transients of up to 250 Hz. This temporal resolution is sufficient for engine development and research applications. The temporal resolution could be further improved by improving the LED throughput (and SNR), as discussed above, and faster signal acquisition, thus enabling use of shorter analysis bins.

The intrinsic sensor speed, independent of gas dynamics associated with the measurement cell, was characterized via temporal resolution measurements, and demonstrated

the fastest transients that the sensor can resolve. Although gas dynamics will certainly limit temporal resolution of the sensor configuration using the measurements cell (see Figure 3), the intrinsic sensor speed is relevant to direct sensor applications; e.g., where the measurement cell is replaced by an engine intake runner for line-of-sight measurements. Moreover, the intrinsic temporal resolution establishes a baseline performance standard that can be used as a reference for assessing sensor improvements. For these experiments, the combined LED beam was modulated from 25 Hz to 400 Hz using a ten-window optical chopper with various layers of polymer (polypropylene office material, Scotch tape, etc.) placed over three of the ten windows as shown in Figure 5. As the chopper rotates, it effectively turns the LED beam on and off via the open and solid portions of the wheel, respectively, and the polymer-covered windows simulate absorption; it is known that the polymer has broad absorption features around the 3.6 μm reference LED emission region. Of course, the intrinsic sensor response is independent of the specific LED used for the assessment, and so the same response would be measured if real or synthetic absorption occurred at the CO_2 or CO wavelengths.

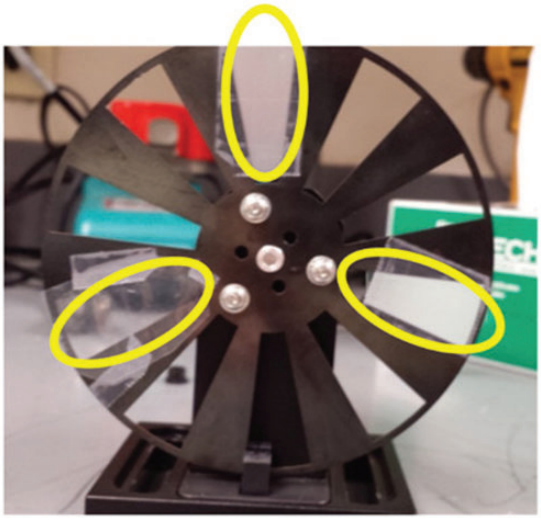

Figure 5. Optical chopper used for beam modulation in the temporal response studies, with three windows covered with various layers of polymer sheet to simulate absorption (highlighted in yellow).

Discussion

The CO_2 and CO calibration curves from the single-gas measurements are shown in Figure 6, along with the 2 sigma (95.4% confidence interval) standard deviation curves. The measurements exhibited low variation between experiments. The non-linear calibration curves are typical of broadband multi-feature absorption,[9] and deviate from the linear response that would be typical of narrow-band (e.g., laser-based) absorption. Although in future work we plan to develop calibrations based on broadband absorption theory, the curves shown in Figure 6 can be used parametrically to convert sensor output to absolute CO_2 and CO concentration levels. The single-gas detection limits, defined as the concentration where the SNR is unity (signal = 2 sigma), were determined to be 30 parts per million (ppm) CO_2 and 400 ppm CO using the 8 cm long measurement cell; changes in the absorption pathlength would inversely scale these detection limit values. Although the intrinsic and secondary (e.g., induced by function generators, etc.) noise was similar for the 4.2 μm (CO_2) and 4.7 μm (CO) LEDs, the 4.2 μm LED had approximately twice the emission power. Thus, the CO_2 measurements have a correspondingly lower SNR and lower detection limit; since the signal is also influenced by spectral and LED parameters in relation to the sensitivity discussion below, the detection limit gain (i.e., 30 ppm versus 400 ppm) is much greater than the power difference between the two LEDs.

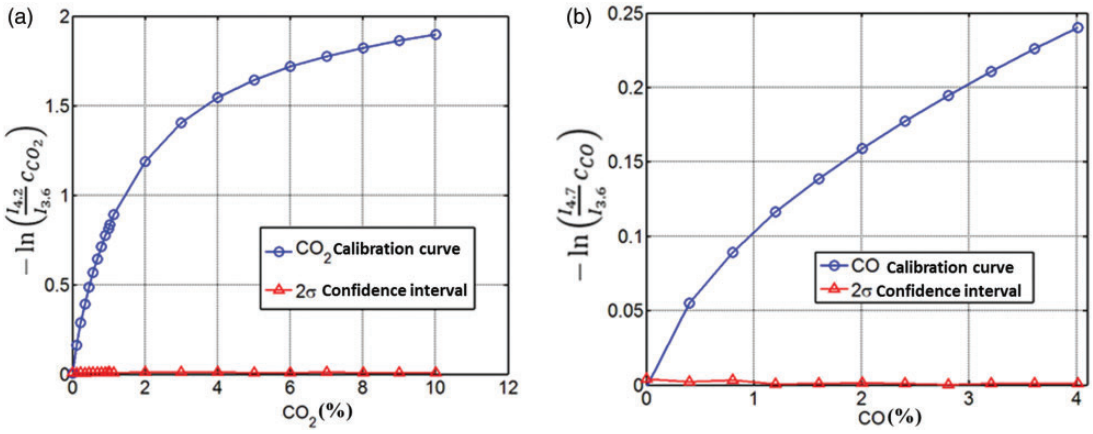

Figure 6. Calibration results for (a) CO_2 and (b) CO in the 8 cm calibration cell. Values of $-\ln((I/I_0)c_i)$ are plotted against the controlled feed CO_2 and CO concentrations.

The measurement sensitivity is indicated by the local slope of the calibration curves shown in Figure 7, which indicates that the sensor is more sensitive to CO_2 than to CO throughout the CO calibration range. The difference in sensitivity and detection limit between the two gases is attributed to the probed spectral absorption features and the nature of the LED filter. As shown in Figure 2, the CO_2 absorption features are much stronger than those of CO, and the spectra and LED filter bandwidth are such that a greater number of CO_2 absorption features are measured compared to CO. This causes the sensor's CO_2 sensitivity to be greater than that for CO. Figure 2 shows that many long-wavelength CO transitions within the 4.7 μm LED emission were rejected by the bandpass filter; the CO sensitivity could be correspondingly improved by using a different filter that incorporated these additional transitions into the CO measurement. For typical narrow-band absorption the sensitivity would be approximately constant and would be proportional to the spectral absorption coefficient of the targeted transition. The decreasing sensitivity with increasing concentration is due to the stronger transitions becoming saturated; as saturation progresses, the specific absorption changes per unit concentration change goes to zero, resulting in the continuously degraded sensitivity. In contrast to the CO_2 behavior in Figure 7, the sensor's CO sensitivity is nearly constant above approximately 1.5%, which is consistent with the measurement being based on weaker absorption features and specifically fewer lines in the saturation regime.

Figure 8 highlights the lack of cross interference between the CO_2 and CO measurements, by overlaying the single-gas calibration curves with those from the stepped and constant cross-interference measurements. Any cross-interference between CO_2 and CO would cause the observed signals for each to diverge from the single-gas calibration results. However, Figure 8 indicates excellent agreement between the various calibration results, and no practical cross-interference for either CO_2 or CO.

In addition to the laboratory-based sensitivity, detection limit, noise, and cross-interference addressed here, engine applications require additional considerations including background IR interference, interference from other combustion products such as nitrous oxide (N_2O), and vibration-induced noise. The frequency-based analysis procedure would aid in rejecting some interference and noise sources that are possible in actual engine experiments, as signals at frequencies other than those specified for the LED modulation are rejected. Thermal emissions from a hot engine surface would most likely be at too low a frequency to affect the measured signal; such thermal IR background would primarily be relevant in a probe-based sensor configuration.[9] Another approach that has been used to address background interference is to directly measure the background by momentarily turning off the LEDs and implementing an offset correction. Figure 1 shows that N_2O has absorption features of comparable magnitude to and overlapping those of CO and CO_2, and is thus a source of potential interference. Nitrous oxide emissions are practically negligible in the internal combustion engine exhaust compared to the percentage levels of CO and CO_2, although N_2O can be produced in catalytic exhaust treatment devices. Nevertheless, potential cross-interference due to absorption from N_2O and other combustion products may be mitigated by using a narrower bandpass filter centered over the 4.8 μm band of the CO

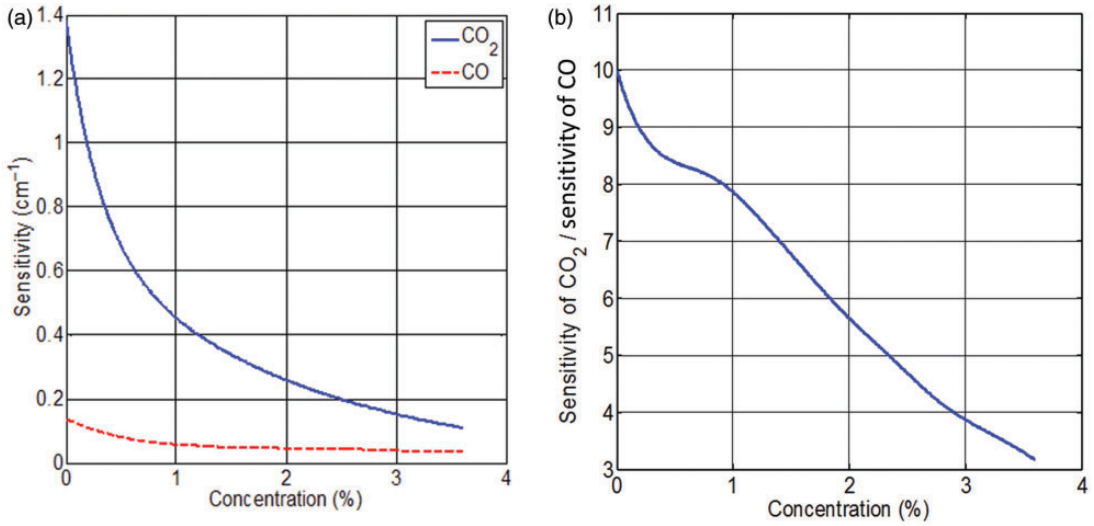

Figure 7. Sensitivity analysis of CO and CO_2, based on the local slope of the calibration curves in Figure 6. (a) Sensitivity of each species, defined as the derivative of the negative natural log of the transmissivity with respect to concentration; (b) ratio of the sensitivity of CO_2 to the sensitivity of CO. At the lower end CO_2 is 10× more sensitive than CO.

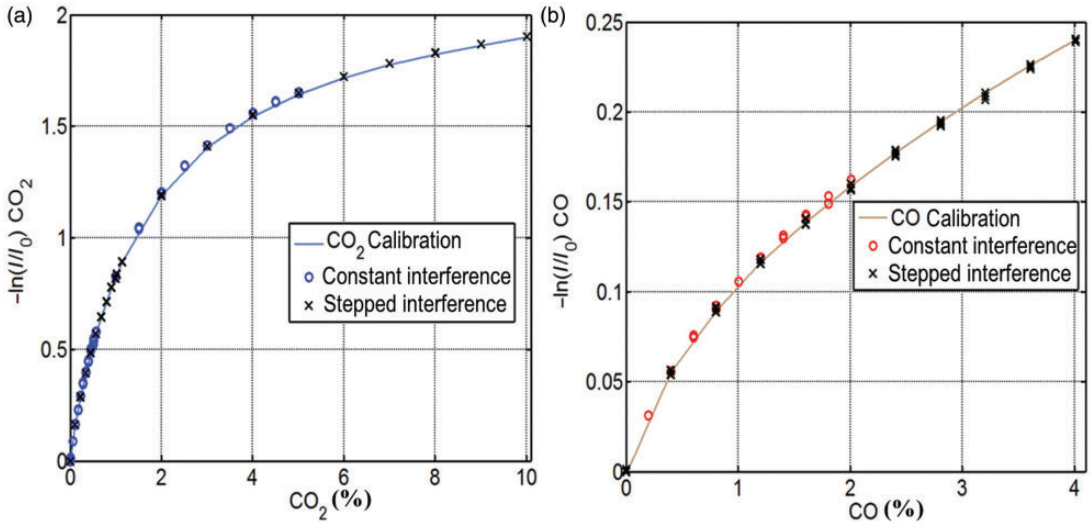

Figure 8. Results from the cross-interference measurements. (a) CO_2; (b) CO. The single-gas calibration curves (Figure 6 data) are plotted as lines, while results from the constant and stepped interference experiments are indicated as circle and crosses, respectively. The error bars for the data points are smaller than the symbols used in the plot. The various calibration results are practically coincident, indicating no practical cross-interference between CO_2 and CO.

absorption. Vibrations should not impact upon the performance of a well-designed and mechanically stable diagnostic based on extractive sampling, such as that of the current sensor, e.g., see Figure 3. In separate work using a similar sensor designed to measure CO_2, it has been observed that the vibration of hollow waveguides used for probe-based on-engine measurements increased the uncertainty in measurements from 0.1% in vibration-free laboratory calibrations to 1.1%; however, these uncertainties were much less than the actual CO_2 concentration fluctuations and did not limit the practical application of the diagnostic.[9] We expect that vibrations would affect a probe-based configuration of the current sensor's performance similarly.

Figure 9 shows results of the temporal response measurements to indicate resolution sufficient for intra-cycle-resolved engine measurements. The high signal peaks are associated with the seven open chopper wheel windows in Figure 5, the zero-signal points are associated with the 10 solid windows, and the intermittent-signal peaks with the three polymer-covered windows that synthesized absorption. The magnitude of the intermediate peaks reflects the number of polymer layers covering each chopper window, with lower signal level indicating greater number of absorbing layers. The clear 2-3-2 temporal pattern of the high-signal peaks reflects the spatial geometry of Figure 5, and can be used to assign the intermediate peaks to specific windows. Specifically, the intermediate peaks surrounding the three high-signal peaks are the two lower circled windows in Figure 5 surrounding the three open chopper windows. Moreover, these two intermediate peaks have the greatest (~1 a.u.) and least (~0.35 a.u.) intermediate signal level, indicating the least and greatest number of absorbing polymer layers, respectively. Correspondingly, the middle (~0.6 a.u.) intermediate signal corresponded to the chopper window opposite the three open windows, and had the intermediate number of absorbing polymer layers. This logical interpretation of the patterns in Figure 8 was consistent with the actual configuration of the chopper (i.e., number and distribution of absorbing layers), and is evidence of the sensor's temporal resolution beyond the ability to resolve individual chopper-window events. At 250 Hz modulation, a chopper window should pass the LED beam every 4 ms, which is consistent with the results shown in Figure 9a. This corresponds to 24 crank-angle-degrees (CAD) for an engine operating at 1000 rev min^{-2}, and indicates the ability to resolve transients on the order of individual (intake or exhaust) valve events. While the experiments performed do not account for sources of interference that may be present in actual engine measurements, the results illustrate that the sensor has sufficient temporal resolution for resolving cylinder-to-cylinder and cycle-to-cycle variations in intake charge and combustion completion; combustion uniformity can be accessed via intake manifold measurements,[9] and combustion-completion fluctuations could be assessed via CO–CO_2 ratio variations.

Faster transients could be resolved with alternate analysis bin size or higher data acquisition unit (DAQ) speed . The 250 Hz modulation results in Figure 9a indicate measurements are below the Nyquist limit and are synchronous with the measurement rate; in this synchronous case, there are exactly four measurements per modulation cycle resulting in consistent signals for the various open-window peaks. Figure 9b demonstrates the nature of transitioning beyond faithful transient characterization. Although 325 Hz

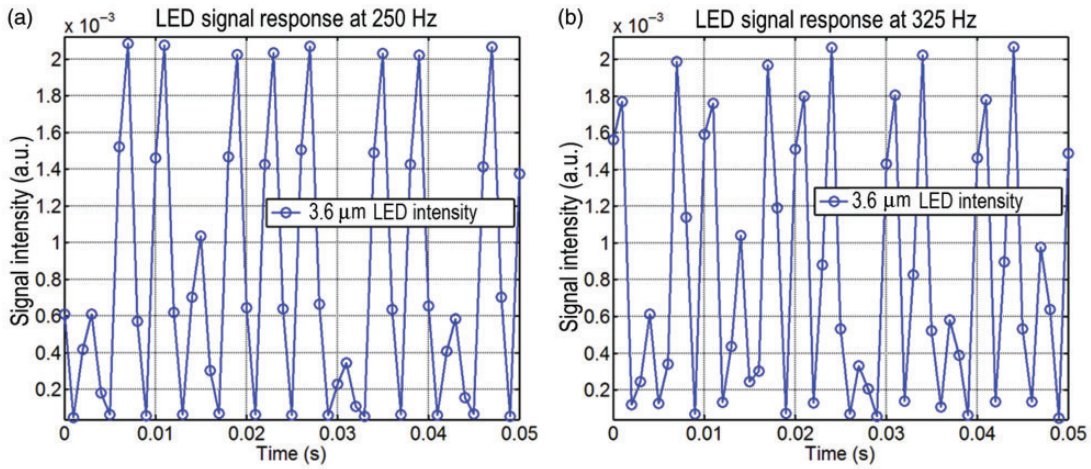

Figure 9. Temporal resolution measurement results for LED modulation. (a) 250 Hz; (b) 325 Hz.

modulation is below the Nyquist limit, and the results clearly show the patterns of the open and synthetic-absorption windows, the transients show more temporal variations compared to the 250 Hz results. This is due to the nonsynchronous analysis and modulation; specifically, at 325 Hz, there are ~3.08 measurements per modulation cycle, causing the measurements to progressively walk through the modulations. This is manifested by the varying peak heights through the chopper revolution. For instance, the open-window high-signal-level peaks vary in magnitude because different points around the modulation peaks are sampled in this nonsynchronous mode. Similarly, there are differences in transient shape for identical transients in subsequent chopper modulations; e.g., the high-peak pair around 0.009 s and 0.042 s in Figure 9b corresponds to the same chopper window, as does the intermediate peak at ~0.013 s and 0.048 s. This demonstrates the onset transient-response error, and such transient distortion would continue with increasing modulation rate until it was completely unresolved at the Nyquist limit. While the sensor has been demonstrated as having sufficient temporal resolution for engine research applications, the temporal resolution could be further extended by increasing the measurement rate. This could be implemented by increasing the DAQ rate or modifying the analysis procedure to use smaller temporal analysis bins; e.g., the temporal resolution could be doubled to 2 kHz by using 500 rather than 1000 data points per FFT analysis bin. Although the signal, noise and other practical tradeoffs would have to be considered, this provides a general framework for further extending the sensor temporal resolution.

Conclusions and Future Work

A sensor for simultaneous detection of CO and CO_2 was developed using low-cost LEDs. The sensor was able to detect concentration changes as small as 30 ppm and 400 ppm for CO_2 and CO, respectively, with no cross-interference between CO_2 and CO. Temporal response measurements indicated that the sensor can resolve fast transients of up to 250 Hz, which is sufficient to resolve cylinder-to-cylinder and cycle-to-cycle variations in an engine operating at 1000 rev min^{-2}, assuming that the implementation of the sensor effectively mitigates the interference from operating in an actual engine environment. This sensor provides the potential to be implemented for on-board monitoring, diagnostics, and control of performance fluctuations associated with these CO and CO_2, including EGR, and combustion completion and stability. The method and design developed here is applicable for developing sensors for a variety of gases, as a number of important gases, such as NO_2, N_2O, and CH_4, have fundamental absorption bands in the MIR spectral region.

Several insights were gained regarding increasing the sensor's detection limit, sensitivity, and temporal resolution. The CO_2 sensitivity was up to ten times greater than CO because a greater number of CO_2 absorption features were measured by the broadband measurement. However, the CO_2 sensitivity degraded much faster than CO (although CO_2 sensitivity remained greater throughout) at higher concentrations because the stronger CO_2 absorption transitions entered saturation before the weaker CO transitions. The CO sensitivity and detection limit could be improved without compromising the cross-interference performance by using a broader LED bandpass filter that incorporated the longer-wavelength CO_2 absorption transitions (in the ~4.7–5 μm region) clipped by the current filter. Temporal resolution could be further improved by using higher DAQ speeds and/or reducing the FFT analysis bin size; this could be further enabled by increasing the sensor SNR by increasing LED emission throughput via improved optical design. Nevertheless, the LED sensor has demonstrated performance for advancing engine and combustion research in its existing state, and these insights provide a pathway for further expanding the range of applicability.

Acknowledgments

Research at UCF was supported by financial assistance from the Federal Aviation Administration Center of Excellence for Commercial Space Transportation (FAA COE-CST) with Ken Davidian and Nickolas Demidovich as program managers, Florida Space Institute, Duke Energy, the UCF Mechanical and Aerospace Department, and the UCF Office of Research and Commercialization. The authors would like to acknowledge travel support provided by the ORAU. Z.L. thanks NSF and DOE SULI for partially supporting this effort. The Oak Ridge National Laboratory research was sponsored by the US Department of Energy, Office of Energy Efficiency and Renewable Energy, Vehicle Technologies Office, with Gurpreet Singh, Ken Howden, and Leo Breton as the program managers.

Conflict of Interest

The authors report there are no conflicts of interest.

Funding

This work was supported by the Federal Aviation Administration Center of Excellence for Commercial Space Transportation (FAA COE-CST), the UCF Mechanical and Aerospace Department, the UCF Office of Research and Commercialization, NSF, DOE SULI, and the US Department of Energy, Office of Energy Efficiency and Renewable Energy, Vehicle Technologies Office.

References

1. US Department of Energy. "International Energy Outlook 2013". 2013. http://www.eia.gov/forecasts/ieo/pdf/0484(2013).pdf [accessed March 18 2016].
2. M. Zheng, G.T. Reader, J.G. Hawley. "Diesel Engine Exhaust Gas Recirculation – A Review on Advanced and Novel Concepts". Energy Convers. Manage. 2004. 45(6): 883–900.
3. R.D. Reitz. "Directions in Internal Combustion Engine Research". Combust. Flame. 2013. 160(1): 1–8.
4. D. Schmeling, J. Bosbach, C. Wagner. "Simultaneous Measurements of Temperature and Velocity Fields in Conective Air Flows". Meas. Sci. Technol. 2014. 25(3): 617–622.
5. H. Teichert, T. Fernholz, V. Ebert. "Simultaneous In Situ Measurement of CO, H_2O, and Gas Temperatures in a Full-Sized Coal-Fired Power Plant by Near-Infrared Diode Lasers". Appl. Opt. 2003. 42(12): 2043–2051.
6. W. Ren, A. Farooq, D.F. Davidson, R.K. Hanson. "CO Concentration and Temperature Sensor for Combustion Gases Using Quantum-Cascade Laser Absorption near 4.7 μm". Appl. Phys. B: Lasers Opt. 2012. 107(3): 849–860.
7. A. Farooq, J. Jeffries, R.K. Hanson. "CO_2 Concentration and Temperature Sensor for Combustion Gases Using Diode-Laser Absorption near 2.7 μm". Appl. Phys. B: Lasers Opt. 2008. 90(3–4): 619–628.
8. L.S. Rothman, I.E. Gordon, Y. Babikov, A. Barbe, D.C. Benner, P.F. Bernath, M. Birk, L. Bizzocchi, V. Boudon, L.R. Brown, A. Campargue, K. Chance, E.A. Cohen, L.H. Coudert, V.M. Devi, B.J. Drouin, A. Fayt, J.M. Flaud, R.R. Gamache, J.J. Harrison, J.M. Hartmann, C. Hill, J.T. Hodges, D. Jacquemart, A. Jolly, J. Lamouroux, R.J.L. Roy, G. Li, D.A. Long, O.M. Lyulin, C.J. Mackie, S.T. Massie, S. Mikhailenko, H.S.P. Müller, O.V. Naumenko, A.V. Nikitin, J. Orphal, V. Perevalov, A. Perrin, E.R. Polovtseva, C. Richard, M.A.H. Smith, E. Starikova, K. Sung, S. Tashkun, J. Tennyson, G.C. Toon, V.G. Tyuterev, G. Wagner, H. Müller, M. Smith. "The HITRAN2012 Molecular Spectroscopic Database". J. Quant. Spectrosc. Radiat. Transfer. 2013. 130: 4–50.
9. J. Yoo, V. Prikhodko, J.E. Parks, A. Perfetto, S. Geckler, W.P. Partridge. "Fast Spatially-Resolved EGR Distrubution Measurements in an Internal Combustion Engine using Absorption Spectroscopy". Appl. Spectrosc. 2015. 69(9): 1050–1061.
10. Radiant. "Zemax". http://www.zemax.com. [accessed Dec 27 2015].